PHYSICAL REVIEW B **94**, 115109 (2016)

Raman and crystal field studies of Tb-O bonds in $TbMn_2O_5$

S. Mansouri,[1,*] S. Jandl,[1] M. Balli,[1] J. Laverdière,[2] P. Fournier,[1] and D. Z. Dimitrov[3,4]
[1]*Regroupement Québécois sur les Matériaux de Pointe et Institut Quantique, Département de Physique, Université de Sherbrooke, Sherbrooke, Canada J1K 2R1*
[2]*Centre Énergie, Matériaux et Télécommunications, Institut National de la Recherche Scientifique, Varennes, Canada J3X 1S2*
[3]*Institute of Optical Materials and Technologies, Bulgarian Academy of Sciences, 1113 Sofia, Bulgaria*
[4]*Institute of Solid State Physics, Bulgarian Academy of Sciences, 1784 Sofia, Bulgaria*

(Received 23 June 2016; revised manuscript received 17 August 2016; published 6 September 2016)

We have studied the temperature dependence of $TbMn_2O_5$ Raman-active phonons and its Tb^{3+} crystal field (CF) excitations. Interestingly, the Raman intensities of some phonons are significantly reduced below ∼180 K. Such behaviors are also observed in $HoMn_2O_5$ and YMn_2O_5 systems. A connection between the Raman intensities and the nearest-neighbor mean-square relative displacement σ^2 is established. Also, some of the Tb^{3+} and Ho^{3+} CF excitations become broader below ∼180 K. These results are discussed in terms of the disorder induced by the Tb-O bond splitting.

DOI: 10.1103/PhysRevB.94.115109

I. INTRODUCTION

In recent years, the manganite multiferroics, $R\mathrm{Mn_2O_5}$ and $R\mathrm{MnO_3}$ ($R = \mathrm{Tb},\ldots,\mathrm{Tm}$), have attracted great interest due to their potential use in a wide range of applications, such as magnetically recorded ferroelectric memory [1,2] and magnetic refrigeration [3,4]. Hur *et al.* [2] have observed in $TbMn_2O_5$ a reversible switching of the electrical polarization in relatively low magnetic fields. Also, Balli *et al.* [3,4] have proposed a new concept for the liquefaction of the hydrogen and helium using a giant rotating magnetocaloric effect at low magnetic fields, reported recently in the multiferroic $HoMn_2O_5$ and $TbMn_2O_5$ single crystals. Furthermore, the understanding of the physics behind the $R\mathrm{Mn_2O_5}$ fundamental properties, such as their lattice dynamics, magnetism, and ferroelectricity, would be of great importance in view of their optimization and direct implementation in functional devices.

The ferroelectricity of $R\mathrm{MnO_3}$ ($R = \mathrm{Tb,Dy},\ldots$) manganites is attributed to a noncollinear magnetic order that breaks the inversion symmetry via a Dzyaloshinskii-Moriya interaction [1,5]. In contrast, in $R\mathrm{Mn_2O_5}$ ($R = \mathrm{Tb},\ldots,\mathrm{Tm}$) manganites, the ferroelectricity is induced or improved by a quasicollinear magnetic interaction [2,6–8]. The crystal structure of $R\mathrm{Mn_2O_5}$ is orthorhombic [9,10] where edge-shared $Mn^{4+}O_6$ octahedra are connected along the c axis and pairs of $Mn^{3+}O_5$ pyramids are linked to two $Mn^{4+}O_6$ chains. Nevertheless, there is no consensus on their space group symmetry. Some experimental data suggest a centrosymmetric *Pbam* space group [9] whereas other results unveil that the actual symmetry group is likely to be $Pb2_1m$ [11–14] or Pm [15], giving rise to an electrical polarization along the b axis even at room temperature.

Raman scattering and infrared measurements are sensitive tools in the study of the lattice dynamics and the local atomic displacements in the materials. For example, the 703 $\mathrm{cm^{-1}}$ Raman mode is found to be IR active in $TbMn_2O_5$ at low temperatures, suggesting a lowering of the symmetry of the space group upon cooling [14]. Also, Valdés Aguilar *et al.* [14] have shown that the temperature dependence of a Tb infrared phonon frequency (at ∼98 $\mathrm{cm^{-1}}$) displays anomalies at 150 and 50 K and retraces the commensurate-incommensurate magnetic transition at low temperature. Garcia *et al.* [16] have studied the $R\mathrm{Mn_2O_5}$ (R = Bi, Eu, and Dy) compounds using micro-Raman scattering. They have observed anomalous phonon shifts below $T^* \sim 60-65$ K, in the paramagnetic phase, which can be attributed to a spin-phonon coupling through short magnetic correlations and/or a magnetostriction effect as observed in $BiMn_2O_5$ [17].

The Raman data can be combined with information from the extended x-ray-absorption fine structure (EXAFS) to better understand the local lattice properties of composite materials. Fitting EXAFS data informs on the average near-neighbor distances R, their mean-square relative displacements σ^2 (MSRD), and the coordination numbers N_R [18]. Tyson *et al.* [19,20] have studied by EXAFS the temperature dependence of the $TbMn_2O_5$ local structure. In particular, they have found that the Tb-O bond distribution is clearly resolved into two distinct peaks below ∼180 K (short and long bonds), suggesting nonequivalent Tb sites, away from the *Pbam* structure. The number of short bonds increases as the temperature decreases, matching up the number of long bonds around 65 K. The Gaussian widths σ^2 and positions R were fitted for each bond below 180 K. The σ^2 of the central absorbing atom relative to its neighbors, which appears in the Debye-Waller factor (DW) $\exp(-2k\sigma^2)$, is crucial to the EXAFS analysis and its applications. Knowledge of σ^2 is important for accurate determination of the coordination numbers. Its temperature dependence gives information on the local structural and thermal vibrational disorder. Many experimental and theoretical studies of DW factors have been conducted previously [21–25] and were designed to obtain an effective σ^2 using experimental vibrational spectra.

In this paper, we study the temperature dependence of the Raman-active phonons and the Tb^{3+} crystal field (CF) excitations of $TbMn_2O_5$. For comparison, $HoMn_2O_5$ and YMn_2O_5 are also studied. The $TbMn_2O_5$ crystallographic orientations and their lattice parameters are checked by x-ray diffraction at room temperature. Magnetization measurements of $TbMn_2O_5$ along their a, b, and c axes are also presented.

---

[*] Corresponding author: saber.mansouri@usherbrooke.ca

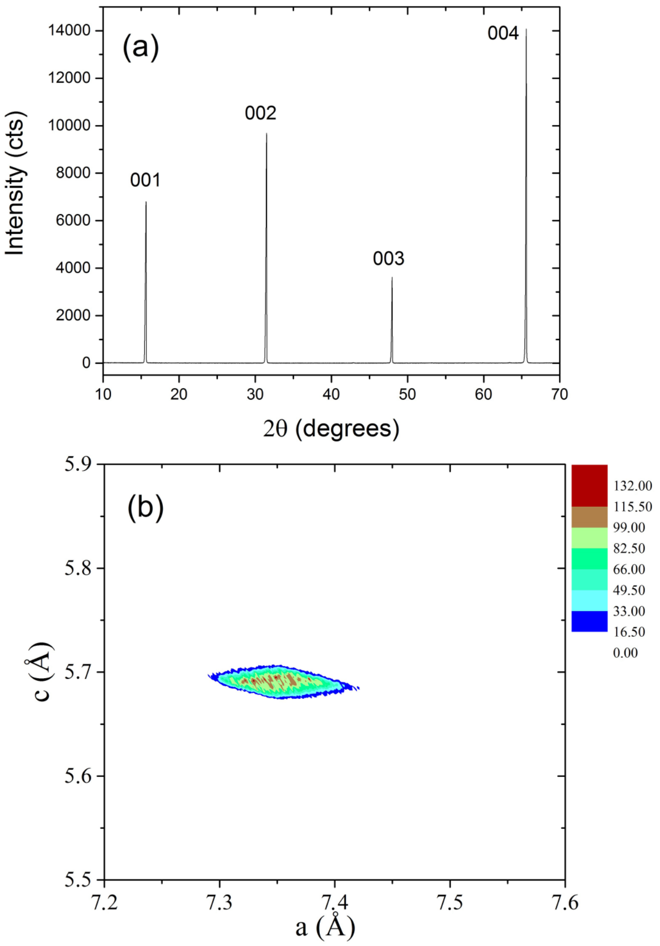

FIG. 1. (a) X-ray diffraction pattern at room temperature of $TbMn_2O_5$ single crystal. (b) An example of reciprocal space mappings for the (102) reflection.

The main objective of this paper is to learn more about the local structural changes in $TbMn_2O_5$ and similar materials that can affect or control their ferroelectric and magnetic properties.

II. EXPERIMENT

$TbMn_2O_5$ single crystals were grown by the high-temperature solution growth method using $PbO\text{-}PbF_2\text{-}B_2O_3$ flux. The $PbO:PbF_2:B_2O_3$ chemical compositions ratios were equal to 0.87:0.12:0.01, respectively. The flux was mixed with $TbMn_2O_5$ powder in a 7:1 ratio and annealed in a platinum crucible at 1225 °C for 48 h in air. After annealing, the temperature was decreased to 1000 °C at a rate of 1 °C/h [26]. Although the main focus of the present paper is on $TbMn_2O_5$, single crystals of YMn_2O_5 and $HoMn_2O_5$ were also studied for comparison. These samples were grown in the same fashion [26,27]. The Raman spectra were measured in the backscattering configuration using a He-Ne laser (632.8 nm) and a Labram-800 Raman spectrometer equipped with an appropriate notch filter and a nitrogen-cooled CCD detector. The Raman spectra were recorded between 300 and 5 K. The samples were mounted on the cold finger of a microhelium Janis cryostat. The exciting laser line was focused through a 50× objective with intensity less than 0.8 mW to avoid local heating. The infrared transmission measurements as a function of temperature were recorded in the $1500\text{--}8000\,\mathrm{cm}^{-1}$ range with a Fourier transform interferometer BOMEM DA3.002 equipped with a quartz-halogen source, a CaF_2 beam splitter, and an InSb detector. The magnetization measurements were carried out using a superconducting quantum interferometer device magnetometer from Quantum Design (SQUID). The lattice parameters of $TbMn_2O_5$ and their orientations were determined by x-ray diffraction technique using D8-Discover x-ray diffractometer from Bruker-AXS with Cu $K\alpha_1$ radiation.

III. RESULTS AND DISCUSSION

An x-ray diffraction (XRD) θ-2θ pattern of a face perpendicular to the c axis of the $TbMn_2O_5$ single crystal is shown in Fig. 1. The presence of (00l) peaks confirms the crystal face orientation, and its high quality with a single domain. Reciprocal space mappings on the (102) and (012)

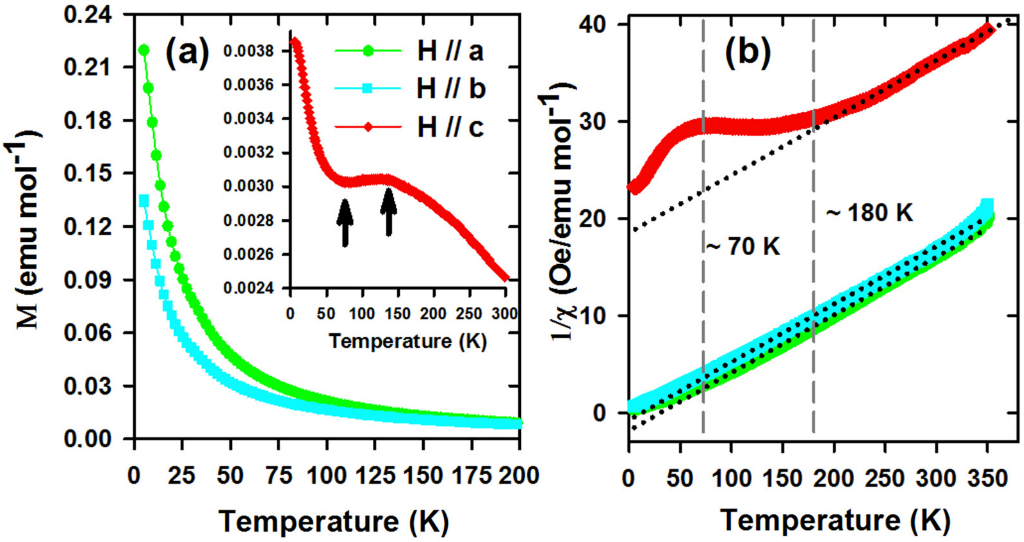

FIG. 2. (a) Temperature dependence of zero-field-cooled (ZFC) magnetization of $TbMn_2O_5$ under a magnetic field of 500 Oe. (b) The inverse susceptibility as a function of temperature fitted to the Curie-Weiss law.

peaks allow us to extract the a and b lattice parameters via their conversion into direct space mappings: An example is shown in Fig. 1(b) for the (102) reflection. The analysis of the room-temperature XRD pattern shows that the single crystal crystallizes in the orthorhombic structure. The room-temperature lattice constants are found to be $a = 7.351$ Å, $b = 8.602$ Å, and $c = 5.690$ Å, in agreement with previous studies [28].

Figure 2(a) presents the temperature dependence of the $\mathrm{TbMn_2O_5}$ single crystal magnetization, measured parallel to the a, b, and c axes under an applied magnetic field of 500 Oe. At very low temperatures, the magnetization along the c axis is markedly smaller than along the ab plane, suggesting that the Tb^{3+} magnetic moment orientation is nearly confined along the ab plane. On the other hand, the thermomagnetic curves along the c axis particularly unveil anomalies at ∼150 and 70 K. These features indicate the complex magnetic behavior in the paramagnetic temperature range. The anomaly at ∼150 K coincides with the Tb-O splitting bonds [19] whereas the anomaly at $T^* \sim 70$ K is a precursor effect of the magnetic order of the Mn moments at $T_N \sim 42$ K and reflects strong magnetic correlations in the paramagnetic phase [16,17]. The inverse magnetic susceptibility ($1/\chi$) as a function of temperature along the easy, middle, and hard axes is plotted in Fig. 2(b). Above T_N, the inverse susceptibility follows the Curie-Weiss law $1/\chi = T/C - \theta/C$ (dashed lines). The deduced effective magnetic moment value is found to be $\mu_{\rm obs} \approx 11.60\,\mu_B$, in good agreement with the theoretical value given by $\mu_{\rm eff} = \sqrt{\mu^2_{\rm eff}(\mathrm{Tb}^{3+}) + \mu^2_{\rm eff}(\mathrm{Mn}^{3+}) + \mu^2_{\rm eff}(\mathrm{Mn}^{4+})^2} = 11.55\mu_B$. The large negative value of the paramagnetic Curie-Weiss temperature $\theta_{\rm CW} \sim -312$ K, along the c axis, implies strong antiferromagnetic interactions, while the large ratio of $|\theta_{\rm CW}|/T_N \sim 7$ indicates a strong spin frustration. In addition, at temperatures below 180 K for which the Tb-O bond splitting occurs, $1/\chi$ starts to deviate significantly from the Curie-Weiss behavior. This clearly demonstrates that the magnetic properties of $\mathrm{TbMn_2O_5}$ are sensitive to the dynamics of the Tb-O bonds.

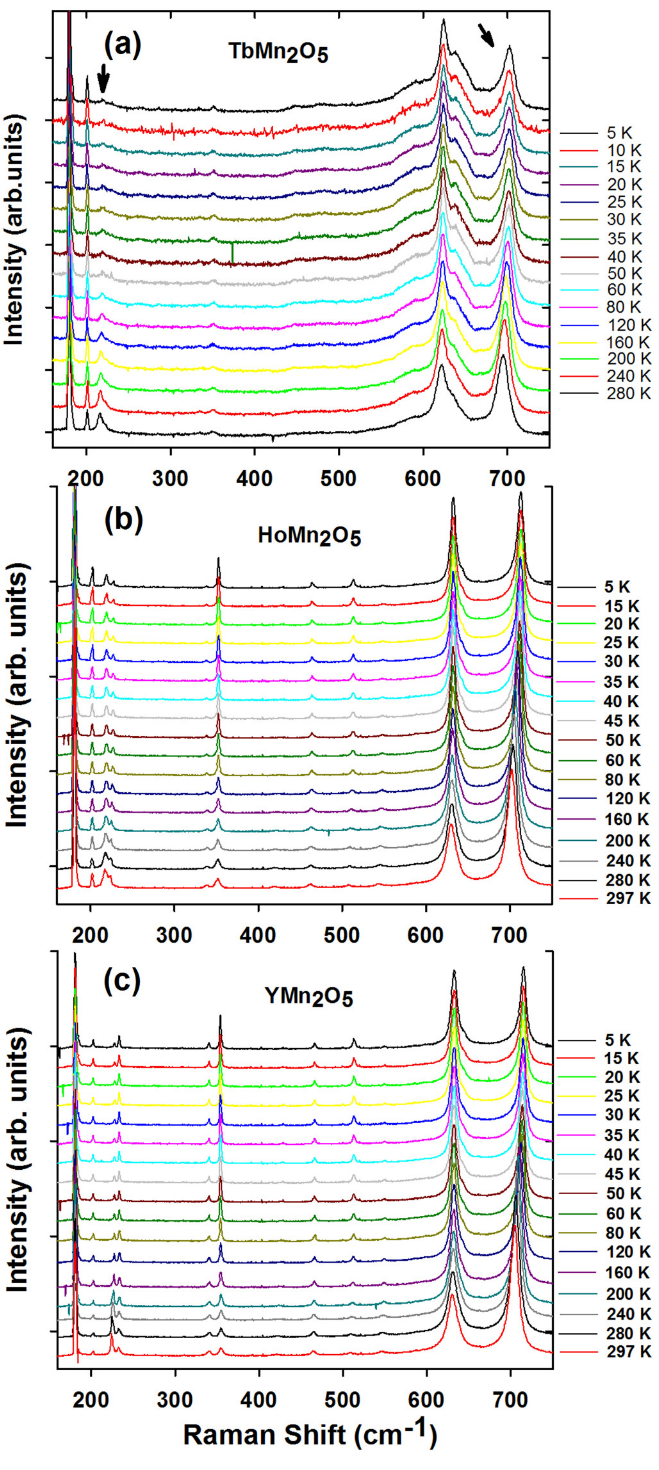

FIG. 3. The temperature dependence of the Raman spectra of (a) $\mathrm{TbMn_2O_5}$, (b) $\mathrm{HoMn_2O_5}$, and (c) $\mathrm{YMn_2O_5}$ in the zz scattering configuration between 297 and 5 K.

Vibrational spectroscopy informs on the local structural properties of materials based on the characteristics of the phonon peaks (frequencies, widths, and intensities). Most of the spectroscopic studies focus only on the evolution of phonon frequencies and widths and rarely consider the behavior of the intensities. The peak intensities are a function of the polarizability and the symmetry, which enables one to probe the bonding covalence and the local structural environment. In this work, we mainly focus on the temperature dependence of the phonon intensities. Figure 3 shows the temperature dependence of the Raman spectra of $\mathrm{TbMn_2O_5}$ [Fig. 3(a)], $\mathrm{HoMn_2O_5}$ [Fig. 3(b)], and $\mathrm{YMn_2O_5}$ [Fig. 3(c)] in the zz polarization configuration. All Raman spectra are recorded under the same experimental conditions and in the same region of the crystal. Detailed polarized Raman spectra of $\mathrm{TbMn_2O_5}$ have been recently reported in Ref. [29]. In particular, the Raman frequency and intensity of the ∼327 $\mathrm{cm^{-1}}$ mode (observed in the B_{1g} symmetry) increase between 300 and 200 K and decrease slightly below ∼160 K [Fig. 4(a)]. A similar behavior is observed in the Raman spectra of $\mathrm{HoMn_2O_5}$ and $\mathrm{YMn_2O_5}$ compounds and is summarized in Fig. 4(a) for the same mode. The displacement pattern of this mode involves an asymmetric bending due to the $\mathrm{O_2}$ (oxygen atoms connecting adjacent Mn^{4+} sites) and Mn^{3+} displacements [30]. Figures 4(b) and 4(c) compare the temperature evolution of the Raman intensities of the ∼220 and ∼700 $\mathrm{cm^{-1}}$ modes of $\mathrm{TbMn_2O_5}$, $\mathrm{HoMn_2O_5}$, and $\mathrm{YMn_2O_5}$. The ∼700 $\mathrm{cm^{-1}}$ mode involves the motion of the $\mathrm{O_3}$ and $\mathrm{O_4}$ oxygen ions connecting the Mn^{3+} and Mn^{4+} bonds whereas the ∼220 $\mathrm{cm^{-1}}$ mode

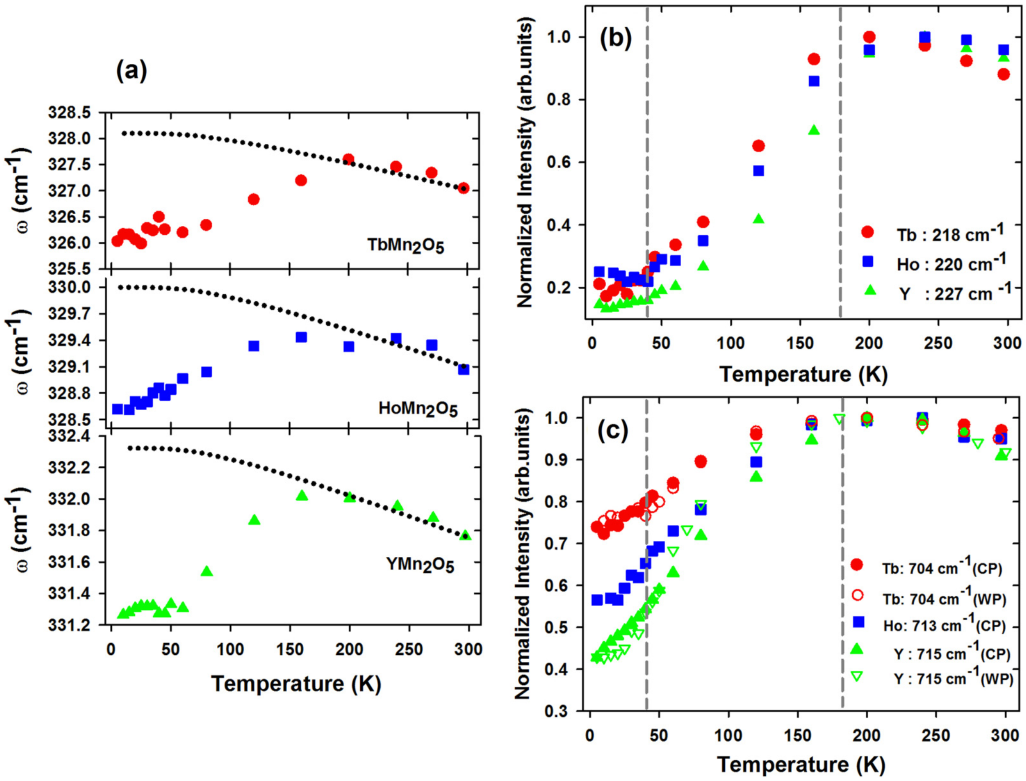

FIG. 4. (a) Thermal evolution of the Raman frequency of the ~327 cm^{-1} mode in TbMn$_2$O$_5$, HoMn$_2$O$_5$, and YMn$_2$O$_5$. Temperature dependence of the Raman intensities of the (b) ~220 cm^{-1} and (c) ~700 cm^{-1} modes of RMn$_2$O$_5$ (R = Tb, Ho, and Y) in the zz scattering configuration. CP and WP indicate cooling and warming processes, respectively.

involves the motion of the R (Tb^{3+}, Ho^{3+}, and Y^{3+}) ions [30,31]. The Raman intensities of these modes increase between 300 and 200 K but then decrease significantly below ~160 K. Such thermal behavior is a reversible process. The decrease in the Raman intensity reflects a rearrangement of the R-O bond lengths in the RMn$_2$O$_5$ structure. Indeed, it occurs at the onset of the splitting of the Tb-O bonds in TbMn$_2$O$_5$ [19].

In the literature, a connection between the behavior of the Raman intensity and the Debye-Waller factor has been established in disordered solids [23,24]. The temperature dependence of the MSRD σ^2 can be deduced from the evolution of the reduced Raman intensity as a function of temperature [24]. For a better comparison with the phonon density of states, the Raman intensity is usually expressed in a reduced form given by

$$I_R(\omega) = I(\omega)\omega[n(\omega)+1]^{-1}, \tag{1}$$

where $n(\omega)$ is the Bose-Einstein distribution function and $I(\omega)$ is the experimental intensity. The reduced Raman intensity $I_R(\omega)$ can be approximated by the product of the density of vibrational states $\rho_R(\omega)$ and a matrix element $R(\omega)$ term leading to $I_R(\omega) = \rho_R(\omega)R(\omega)$. According to Lottici [24], a best fit for the phonon density of states is usually looked for with $R(\omega) = \omega^n$ ($n = 1,2,\ldots$). For disordered materials [23,24], the nearest-neighbor MSRD is then given by

$$\sigma_R^2 = \frac{\hbar}{2\mu}\int \frac{I_R(\omega)}{\omega R(\omega)} \coth\left(\frac{\hbar\omega}{2k_BT}\right) d\omega, \tag{2}$$

where μ is the reduced mass of the atomic pair and k_B is the Boltzmann constant. In order to verify whether the temperature dependence of the Raman intensities is connected to the nearest-neighbor MSRD σ^2 of the Tb-O bonds deduced from the EXAFS experimental data, σ_R^2 was determined from the TbMn$_2$O$_5$ Raman spectra. We consider only the Raman-active modes that are sensitive to the Tb-O bond splitting, such as the phonon modes at 218 and 704 cm^{-1} and their corresponding partial phonon density of states. Best fit is obtained here with $R(\omega) = \frac{1}{2}\omega^2$. The calculation results are shown in Fig. 5. The temperature dependence of σ_R^2 (Tb-O), obtained from the Raman data, is in agreement with that of $\sigma_{\mathrm{EXAFS}}^2$ (Tb-O) as deduced from the EXAFS experimental results. Our findings confirm the local lattice distortion of the TbO$_8$ polyhedra. Additionally, this local structural change should be present in HoMn$_2$O$_5$ and YMn$_2$O$_5$ as a universal behavior of the lattice dynamic properties of the RMn$_2$O$_5$ multiferroics.

The temperature dependence of the rare-earth CF excitations also provides useful information about the surrounding ligands and local inhomogeneities. In the literature, there is no information about the Tb^{3+} crystal field scheme for TbMn$_2$O$_5$. Figure 6 shows the Tb^{3+} $(4f^8)F_6 \rightarrow F_5$, F_4, F_3, F_2, and F_1 CF transitions at 4.2 K for **E** parallel to the a axis, b axis, and ac plane. Each ^2F_J multiplet corresponds to $2J+1$ sublevels. The temperature dependence of the Tb^{3+} CF excitations, for **E** parallel to the ab plane, shows that some absorption bands disappear at low temperatures. These satellites are associated with the F_6 ground-state excited levels 18, 37, 75, 120, 143, 180, 246, and 278(±2) cm^{-1} when

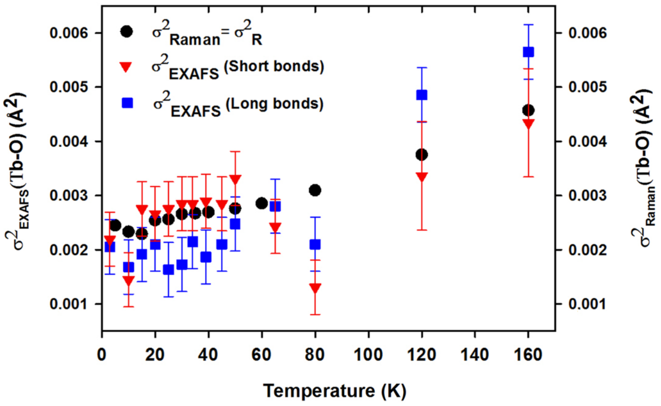

FIG. 5. σ^2 of the Tb-O bonds in $TbMn_2O_5$ as a function of temperature. The squares and triangles are the σ^2_{EXAFS} experimental data obtained by Tyson *et al.* [19], as reported with their corresponding error bars. The solid circles are the results of the calculation of σ^2_R (Tb-O) with the Raman data.

thermally populated. Their energy values are deduced from a comparison between the thermally excited levels of the ^7F_J multiplets ($J = 5$, 4, 3, and 2). The identification of these CF excitations is important to avoid any confusion with other possible low-frequency excitations (electromagnons or phonons). Indeed, our results confirm that the feature around 120 cm^{-1} observed in the infrared phonon spectra of $TbMn_2O_5$ is not a phonon excitation but rather a crystal field level of the Tb^{3+} ion [14]. Furthermore, the imprints of the sublevels around 75, 120, and 143 cm^{-1} are also observed as inflections (gray arrows) in the reflectivity spectrum of $TbMn_2O_5$ (inset of Fig. 6). In addition, the sublevels around 18 and 37 cm^{-1} are observed in optical transmission and inelastic neutron scattering measurements [32,33]. The low-frequency excitation at 18 cm^{-1}, also observed in YMn_2O_5, is identified as an electromagnon [34]. This suggests that, for $TbMn_2O_5$, this excitation has probably a mixed character (electric and magnetic dipole) as has been recently proposed by Sirenko *et al.* [35] for the lowest CF excitations of Ho^{3+} in $HoMn_2O_5$.

Figure 7(a) shows the transmission map of Tb^{3+} $F_6 \rightarrow F_4$ CF transitions. The solid black circles indicate the CF levels of the $^7F_{J=4}$ multiplet and the open circles reflect the thermally populated excited levels of the ground state ($J = 6$). All predicted sublevels for the $^7F_{J=4}$ multiplet (also for $^7F_{J=3}$) are detected: 3393, 3431, 3453, 3484, 3507, 3628, 3656, 3697, and 3721 cm^{-1} (4426, 4462, 4490, 4536, 4550, 4606, and 4633 cm^{-1}). There is no clear doubling of the total number of absorption bands that would confirm unequivocally two Tb^{3+} site symmetries. However, the full width at half maximum (FWHM) of 3393, 3453, and 3697 cm^{-1} CF excitations [Figs. 7(b)–7(d), respectively] becomes larger below ∼180 K, reflecting a local disorder effect induced by the splitting of Tb-O bonds. Their FWHM decreases or becomes nearly constant when the number of the short bonds matches up with the number of the long bonds below 50 K. We speculate that the splitting of Tb-O bonds involves a small deviation of the Tb^{3+} ions from their centrosymmetric site in the *Pbam* space group that manifests in the broadening of some CF excitations. Similar behaviors are also observed for the Ho^{3+} CF excitations in $HoMn_2O_5$ (Fig. 8), suggesting a similar local disorder effect induced by the splitting of Ho-O bonds. This suggests that the dynamics of the *R*-O bond lengths plays a role in the ferroelectric properties of these systems at high

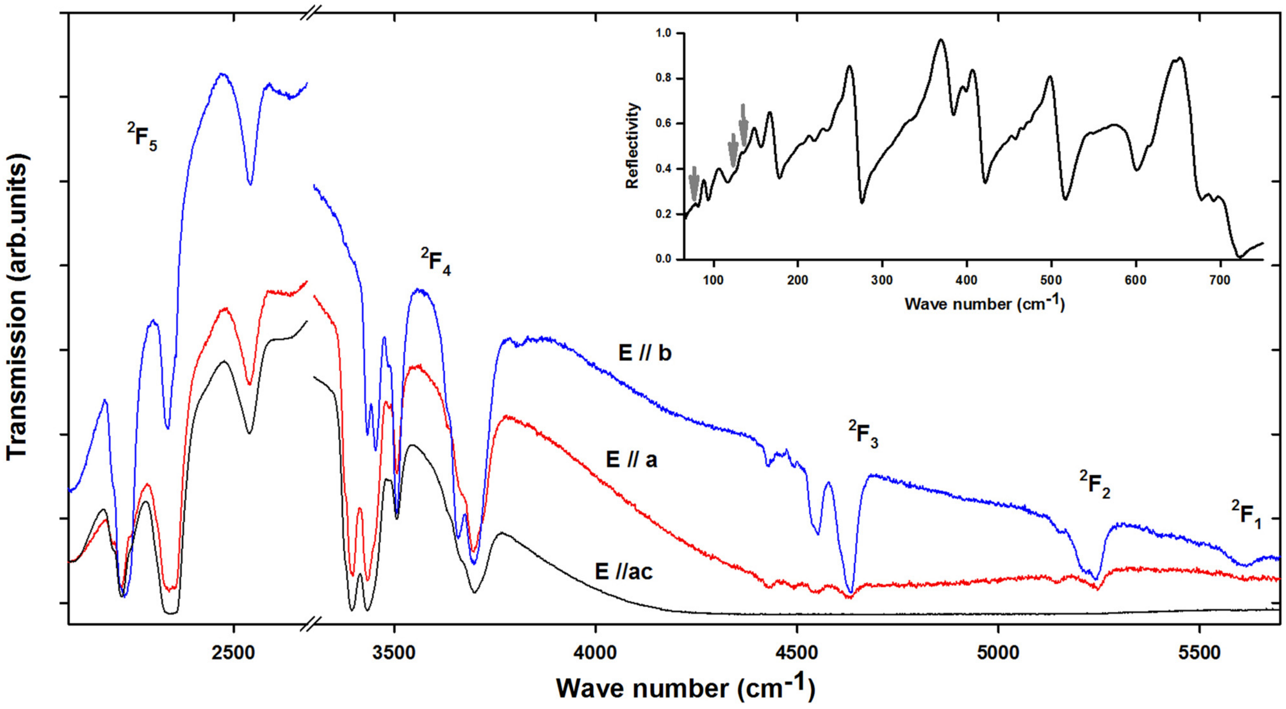

FIG. 6. Transmission spectra of Tb^{3+} $F_6 \rightarrow F_5$, F_4, F_3, F_2, and F_1 CF transitions in $TbMn_2O_5$ at 4.2 K. The inset shows the reflectivity spectrum of $TbMn_2O_5$ at 4.2 K. The Tb^{3+} CF excitations at 75, 120, and 143 cm^{-1} are observed as inflections in the reflectivity spectrum (gray arrows).

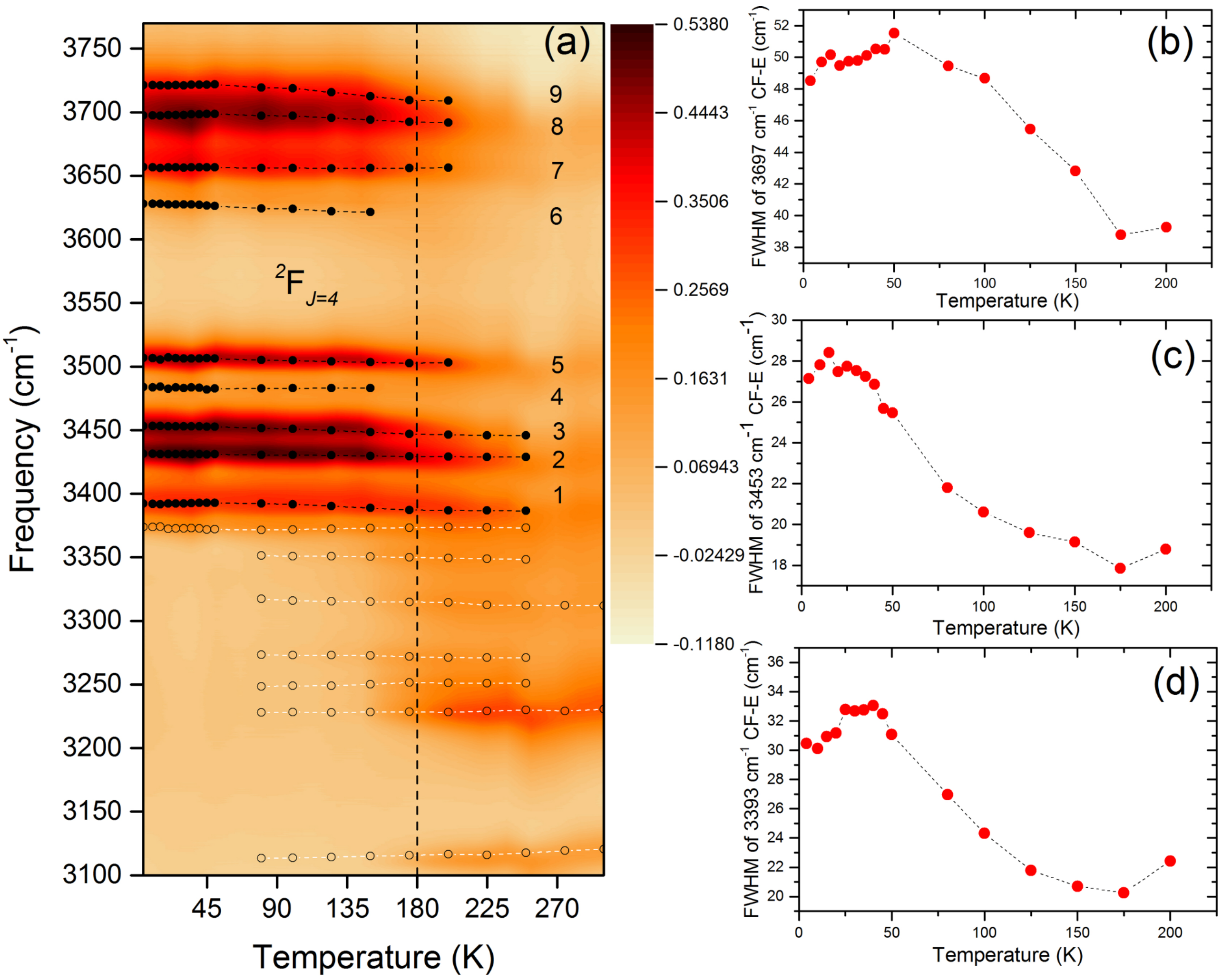

FIG. 7. (a) Transmission maps of Tb^{3+} $F_6 \rightarrow F_4$ CF transitions, where the solid black circles indicate the CF levels of the $^7F_{J=4}$ multiplets and the open black circles trace the excited levels of the ground state ($J = 6$) thermally populated. (b)–(d) show the temperature dependence of the full width at half maximum (FWHM) of the 3697, 3453, and 3393 cm^{-1} CF excitations.

temperature. This relationship between the splitting of the R-O bonds and the loss of inversion symmetry in the RMn_2O_5 systems needs to be further investigated.

Also, the dynamics of the R-O bonds seems to be at the origin of the large dielectric permittivity observed in the paraelectric phase of RMn_2O_5 (R = Tb, Dy, and Er) that becomes significantly important above 200 K and quasiuniform below 180 K [36]. Tyson *et al.* [20] have also reported that the temperature and magnetic field dependences of the Tb-O distribution exhibit changes at low temperature, which are possibly related to the inversion of the electric polarization. All these facts suggest a crucial role of the R-O bond splitting in the ferroelectric properties of the RMn_2O_5 systems.

IV. CONCLUSION

The temperature dependence of the Raman-active phonons and the Tb^{3+} crystal field excitations in $TbMn_2O_5$ are studied. The decrease in the Raman intensities and the frequencies of some $TbMn_2O_5$ phonons below 180 K are attributed to the Tb-O bond splitting. The temperature dependence of the σ^2_{EXAFS} (Tb-O) deduced from the EXAFS data are reproduced with the σ^2_R (Tb-O) as obtained from the reduced Raman intensity. Similar Raman-intensity behaviors are also observed in the RMn_2O_5 (R = Ho, Y) compounds, predicting that the R-O bond splitting is a universal behavior of the RMn_2O_5 dynamic lattice properties. Also, all predicted sublevels of the $^7F_{J=4,3}$ multiplets associated with one site symmetry are detected. There is no evidence for a nonequivalent second site. However, some excitations become broader below ~180 K, reflecting local oxygen arrangements induced by the Tb-O bond splitting and its possible correlation to the ferroelectric properties of the RMn_2O_5 compounds.

ACKNOWLEDGMENTS

We acknowledge the support from the National Science and Engineering Research Council of Canada, the Fonds de Recherche du Québec – Nature et Technologies (FRQNT), and Canada Foundation for Innovation. This research was undertaken owing in part to funding from the Canada First Research Excellence Fund. D.Z.D. acknowledges the INERA REGPOT-2012-2013-1 project support.

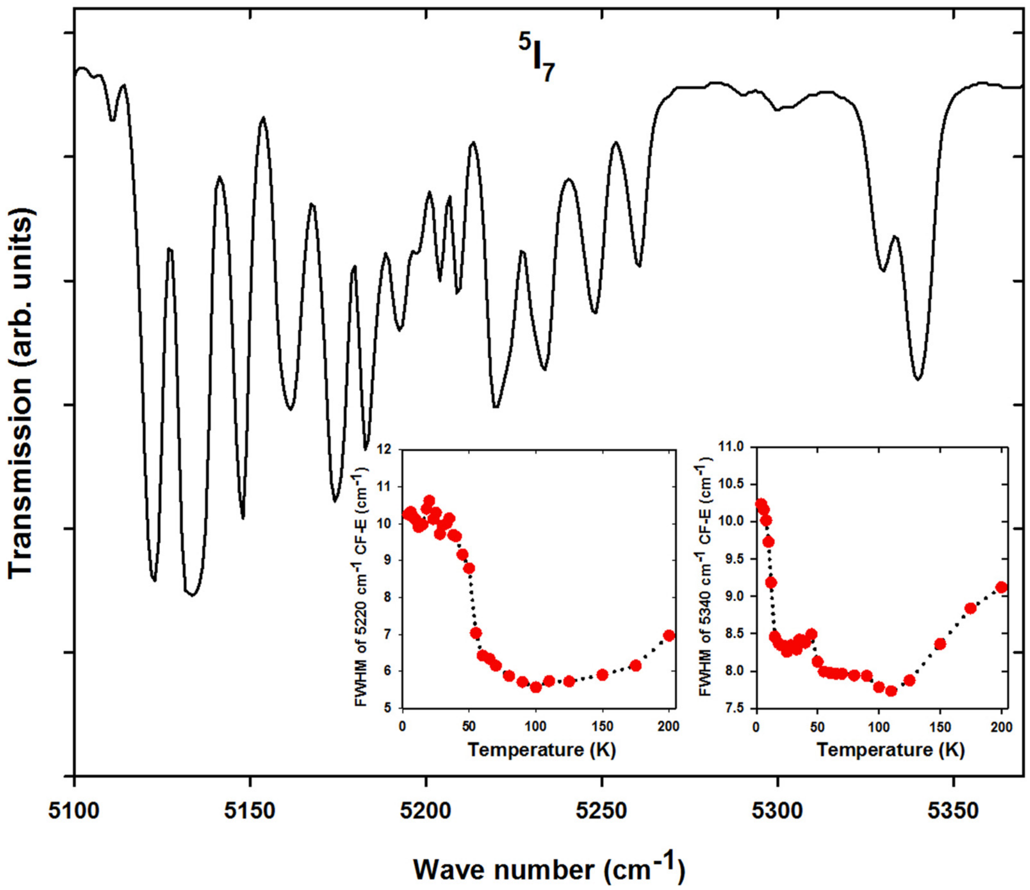

FIG. 8. Transmission spectra of Ho^{3+} $I_8 \rightarrow I_7$ CF transitions in HoMn$_2$O$_5$ at 4.2 K. The insets show the temperature dependence of the FWHM of the 5220 and 5340 cm^{-1} CF excitations.

[1] T. Kimura, T. Goto, H. Shintani, K. Ishizaka, T. Arima, and Y. Tokura, Nature (London) **426**, 55 (2003).

[2] N. Hur, S. Park, P. Sharma, J. Ahn, S. Guha, and S.-W. Cheong, Nature (London) **429**, 392 (2004).

[3] M. Balli, S. Jandl, P. Fournier, and D. Z. Dimitrov, Appl. Phys. Lett. **108**, 102401 (2016).

[4] M. Balli, S. Jandl, P. Fournier, and M. M. Gospodinov, Appl. Phys. Lett. **104**, 232402 (2014).

[5] I. A. Sergienko and E. Dagotto, Phys. Rev. B **73**, 094434 (2006).

[6] S.-W. Cheong and M. Mostovoy, Nature (London) **6**, 13 (2007).

[7] C. Wilkinson, P. J. Brown, and T. Chatterji, Phys. Rev. B **84**, 224422 (2011).

[8] Y. S. Oh, B.-G. Jeon, S. Y. Haam, S. Park, V. F. Correa, A. H. Lacerda, S.-W. Cheong, G. S. Jeon, and K. H. Kim, Phys. Rev. B **83**, 060405(R) (2011).

[9] J. A. Alonso, M. T. Casais, M. J. Martínez-Lope, J. L. Martínez, and M. T. Fernández-Díaz, J. Phys.: Condens. Matter **9**, 8515 (1997).

[10] H. Kimura, S. Kobayashi, Y. Fukuda, T. Osawa, Y. Kamada, Y. Noda, I. Kagomiya, and K. Kohn, J. Phys. Soc. Jpn. **76**, 074706 (2007).

[11] L. C. Chapon, G. R. Blake, M. J. Gutmann, S. Park, N. Hur, P. G. Radaelli, and S.-W. Cheong, Phys. Rev. Lett. **93**, 177402 (2004).

[12] G. R. Blake, L. C. Chapon, P. G. Radaelli, S. Park, N. Hur, S.-W. Cheong, and J. Rodriguez-Carvajal, Phys. Rev. B **71**, 214402 (2005).

[13] I. Kagomiya, S. Matsumoto, K. Kohn, Y. Fukuda, T. Shoubu, H. Kimura, Y. Noda, and N. Ikeda, Ferroelectrics **286**, 167 (2003).

[14] R. Valdés Aguilar, A. B. Sushkov, S. Park, S.-W. Cheong, and H. D. Drew, Phys. Rev. B **74**, 184404 (2006).

[15] V. Baledent, S. Chattopadhyay, P. Fertey, M. B. Lepetit, M. Greenblatt, B. Wanklyn, F. O. Saouma, J. I. Jang, and P. Foury-Leylekian, Phys. Rev. Lett. **114**, 117601 (2015).

[16] A. F. Garcia-Flores, E. Granado, H. Martinho, R. R. Urbano, C. Rettori, E. I. Golovenchits, V. A. Sanina, S. B. Oseroff, S. Park, and S.-W. Cheong, Phys. Rev. B **73**, 104411 (2006).

[17] E. Granado, M. S. Eleotério, A. F. Garcia-Flores, J. A. Souza, E. I. Golovenchits, and V. A. Sanina, Phys. Rev. B **77**, 134101 (2008)

[18] *EXAFS Spectroscopy: Techniques and Applications*, edited by B. K. Teo and D. C. Joy (Plenum, New York, 1981).

[19] T. A. Tyson, M. Deleon, S. Yoong, and S.-W. Cheong, Phys. Rev. B **75**, 174413 (2007).

[20] T. A. Tyson, Z. Chen, M. A. DeLeon, S. Yoong, and S.-W. Cheong, J. Magn. Magn. Mater. **321**, 1714 (2009).

[21] J. J. Rehr and R. Alben, Phys. Rev. B **16**, 2400 (1977).

[22] E. Sevillano, H. Meuth, and J. J. Rehr, Phys. Rev. B **20**, 4908 (1979).

[23] P. P. Lottici and J. J. Rehr, Solid State Commun. **35**, 565 (1980).

[24] P. P. LotticiPhys. Rev. B **35**, 1236 (1987).

[25] G. Dalba and P. Fornasini, J. Synchrotron Radiat. **4**, 243 (1997).

[26] B. Mihailova, M. M. Gospodinov, B. Güttler, F. Yen, A. P. Litvinchuk, and M. N. Iliev, Phys. Rev. B **71**, 172301 (2005).

[27] B. Wanklyn: J. Mater. Sci. **7**, 813 (1972).

[28] L. M. Volkova and D. V. Marinin, J. Phys.: Condens. Matter **21**, 015903 (2009).

[29] S. Mansouri, S. Jandl, B. Roberge, M. Balli, D. Z. Dimitrov, M. Orlita, and C. Faugeras, J. Phys.: Condens. Matter **28**, 055901 (2016).

[30] A. P. Litvinchuk, J. Magn. Magn. Mater. **321**, 2373 (2009).

[31] C. Wang, G.-C. Guo, and L. He, Phys. Rev. B **77**, 134113 (2008).

[32] A. B. Sushkov, R. Valdés Aguilar, S. Park, S.-W. Cheong, and H. D. Drew, Phys. Rev. Lett. **98**, 027202 (2007).

[33] S. Petit, V. Balédent, C. Doubrovsky, M. B. Lepetit, M. Greenblatt, B. Wanklyn, and P. Foury-Leylekian, Phys. Rev. B **87**, 140301(R) (2013).

[34] A. B. Sushkov, M. Mostovoy, R. Valdés Aguilar, S.-W. Cheong, and H. D. Drew, J. Phys.: Condens. Matter **20**, 434210 (2008).

[35] A. A. Sirenko, S. M. O'Malley, K. H. Ahn, S. Park, G. L. Carr, and S.-W. Cheong, Phys. Rev. B **78**, 174405 (2008).

[36] T. C. Han, J. G. Lin, K. M. Kuo, and G. Chern, J. Appl. Phys. **103**, 084106 (2008).